Scientific Research

Application of Texture Measures to Study Effect of B Chromosomes on the 3D Architecture of Plant Chromatin

Hanna Sas-Nowosielska[1*], Jolanta Małuszyńska[1], Tytus Bernas[2,3]

[1]Department of Plant Anatomy and Cytology, Faculty of Biology and Protection of Environment, University of Silesia, Jagiellonska, Poland; [2]Royal College of Surgeons in Ireland, St. Stephens Green, Ireland; [3]Faculty of Biochemistry, Biophysics and Biotechnology, Jagiellonian University, Gronostajowa, Poland.
Email: *h.sasnowosielska@gmail.com

ABSTRACT

Background: Supernumerary chromosomes (B) comprise optional complement to basic (A) chromosome set. The presence of B-chromosomes may significantly reduce plant vigor and fertility. Potentially active genes constitute only small fraction of DNA of these chromosomes indicating that these effects are mediated by epigenetic mechanisms. One example is down-regulation of rDNA genes and condensation of their respective chromatin regions (demonstrated in squashed preparations using 2D microscopy). It may be postulated that the presence of B chromosomes leads to more extensive changes of local chromatin structure. Verification of hypothesis requires studying 3D spatial architecture of intact nuclei in tissue. **Results:** An image processing algorithm was developed and applied for isolation (from the confocal datasets) of regions corresponding to single nuclei. The nuclei were segmented using iterative global thresholding followed by growing and merging of regions belonging to different nuclei. The result of segmentation was verified by a human observer. Chromatin architecture was characterized quantitatively using global fluorescence intensity distribution measures (mean, variance) and local intensity distribution parameters (haraclick features, wavelet energy, runlength features). The sets of parameters corresponding to populations of nuclei with different number of B-chromosomes were subjected to discriminate analysis. The distinct parameters were then correlated with depth in tissue at which a given nucleus was positioned. **Conclusions:** Combination of light microscopy with dedicated image processing and analysis framework made it possible to study chromatin architecture in nuclei containing various number of B chromosomes. These data indicate that alterations of 3D chromatin distribution occur globally in the interphase nuclei in the presence of Bs. The changes occur at the spatial scale comparable with the resolution limit of light microscopy and at larger distances.

Keywords: Sand Tray; Sun Dry; Fungicides; Urea Fertilizer; Plant Population; Growth; Potato Micro-Cuttings

1. Introduction

Supernumerary chromosomes (B), present in a number of plant and animal species [1], are facultative complement of basic chromosome set (A). The B chromosomes are mostly smaller than their counterparts of the A set and their numbers may vary between different organisms in one species or different cells in one organism [2,3] These chromosomes have high content of repetitive DNA sequences and thus may be abundant in constitutive heterochromatin [3-5]. Only small fraction genetic material of B chromosomes contains potentially active genes [3]. In plant organisms known genetic sequences of this kind contain mostly rDNA transcribed to 45S pre-ribosomal rRNA [3,6-10]. The presence of B chromosomes may significantly (usually in a negative way) affect vitality and fertility of an organism [2,11-13]. Interference of B

chromosomes with normal flow of mitosis and meiosis is well documented but little is known about their effects in interphase nuclei. One example is down-regulation of the activity of rDNA genes [8]. B-chromosome effects may be mediated by epigenetic mechanisms. These mechanisms include methylation of DNA and histones as well as acetylation and phosphorylation of the latter [14]. Changes of molecular chromatin structure are accompanied by recruitment of specific proteins and alteration of spatial (3D) chromatin architecture [15,16]. Moreover, the presence of blocks of constitutive heterochromatin may facilitate heterochromatization of potentially active chromatin regions [17,18]. Indeed, condensation of NOR and satellite regions of chromosome 1 in rye in the presence of B chromosomes was reported in [7,8]. Modification of the spatial structure of rDNA loci was described in other studies as well [9]. One may hypothesize that

*Corresponding author.

this effect is not unique to rDNA genes and that the presence of B chromosomes leads to more extensive changes of local chromatin structure [1,8,11,19]. To verify this hypothesis in plants one needs to study spatial (3D) architecture of intact nuclei in tissue.

Cellular morphology may be analyzed in quantitative manner using mathematical descriptors (features) of texture of light micrographs [20,21]. In particular, the texture features have been applied to investigate dependence between chromatin architecture and its functioning [22-25]. However, the spatial (3D) structure of chromatin in plant nuclei containing B chromosomes has not been directly investigated. The majority of currently available data has been obtained from genomic studies or cytological examination of spread metaphase chromosomes or squashed preparations of interphase nuclei by 2D light microscopy [3,8,13].

Therefore, in this study, a plant characterized by simple karyotype (*Crepis capillaris*) [26] was used to study effects of the presence of B chromosomes with 3D light microscopy. Only root meristem regions of this non-polysomatic plant were imaged to eliminate possible influence of karyotype variability other than that connected with the supernumerary chromosomes. Technique of segmentation of nuclei from 3D images of the tissue was developed together with a method for quantification of changes of chromatin architecture. Lastly, statistical techniques were applied to isolate major elements of the postulated changes of chromatin structure and to facilitate biological interpretation of these findings.

2. Methods

2.1. Preparation and Imaging of Biological Material

Crepis capillaris (L.) plants with different number of B chromosomes (2n = 6 + Bs) were use in this study. To have suitable amount of root meristems of each genotype a culture of hairy roots was established. Hairy roots were induced by direct infection of young leaves of *C. capillaris* with *Agrobacterium rhizogenes* according to [27] and four lines of roots with 0 - 3B chromosomes were obtained. The transformed roots were cultured on liquid 1/2 MS medium (Sigma, Poland). The culture was maintained for two years, by passages every 3 weeks to fresh medium. Transformed roots were isogenic, thus each line was a clone of one root and stable at the diploid level even in long-term culture [28,29]. Meristem parts of the roots were fixed (7 days after a passage) in physiological ionic strength and pH (1% formaldehyde in PBS, pH 7.4), and stained with 0.002% DAPI (v/w). The material was mounted in PBS with DAPI on glass slides for microscope imaging.

Series of optical sections (stacks) were registered us-

ing a confocal fluorescence microscope (Olympus FV-1000) equipped with a 60×, 1.2 numerical aperture (NA) PlanApo water-immersion objective, primary dichroic mirror 405/488 nm and a 25 mW diode laser (Coherent BV, the Netherlands). Image registration was optimized so as to eliminate photobleaching while preserving good light penetration depth. Fluorescence of DAPI was excited using 405 nm light and detected in the range 420 - 485 nm. The confocal aperture was set equal to one Airy unit at maximum of DAPI emission. Series of optical sections of 640 × 640 pixels were registered using photon counting at 5 µs/pixel dwell time. The voxel dimensions in the object space were 70 nm in both x and y dimensions and 210 nm in z direction, respectively. Sets of nuclei corresponding to different numbers of B chromosomes were obtained by imaging of 10 to 15 roots for each B variant. Usually from 75 to 200 nuclei could be segmented from a stack (as described further), so the number of nuclei corresponding to each B variant was between 700 and 1300.

2.2. Image Processing and Analysis

Regions corresponding to single nuclei were isolated from the confocal datasets using an image processing routine developed for this task (**Figures 1** and **2**). It should be noted that attenuation of image brightness with depth occurred in the imaged plant tissue (as a result of light absorption and scattering, see **Figure 2(B)**). Therefore, to correct for this effect optical sections were transformed (using piece-wise histogram stretching) sequentially starting from the top (the brightest) so that 5, 25, 50, 75 and 95 percentiles of intensity histogram of a section were identical to the respective values for its predecessor in series.
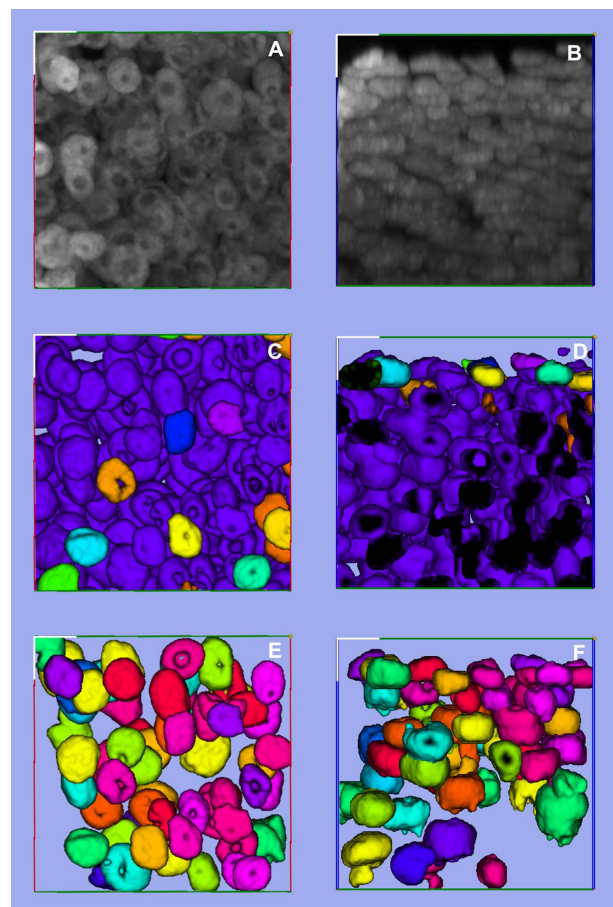
The corrected 3D data sets were subjected to median filtering (3 × 3 × 3 voxel mask) and segmentation in order isolate nuclei (**Figure 1**). First, the binary mask containing all nuclei was calculated using multiple thresholding with Otsu algorithm [20,30,31] where the lowest of the 5 thresholds (minimum signal intensity) was used for global binarization. Since single binarization with this minimal threshold resulted in merging of volumes corresponding to single nuclei (**Figures 2(C)**, **(D)**) an iterative segmentation procedure was used. The stacks were sequentially thresholded starting from the maximum intensity and newly detected pixels were subjected to binary closing. These pixels were assembled in continuous groups (8-connectivity) and labeled (in each step) depending on whether they were adjacent to previously labeled groups (objects). In order to detect adjacency the previously detected objects were dilated 3 times and logical sums with all new groups were calculated. Each new group was combined with the already detected object with the largest non-zero union. The merging was
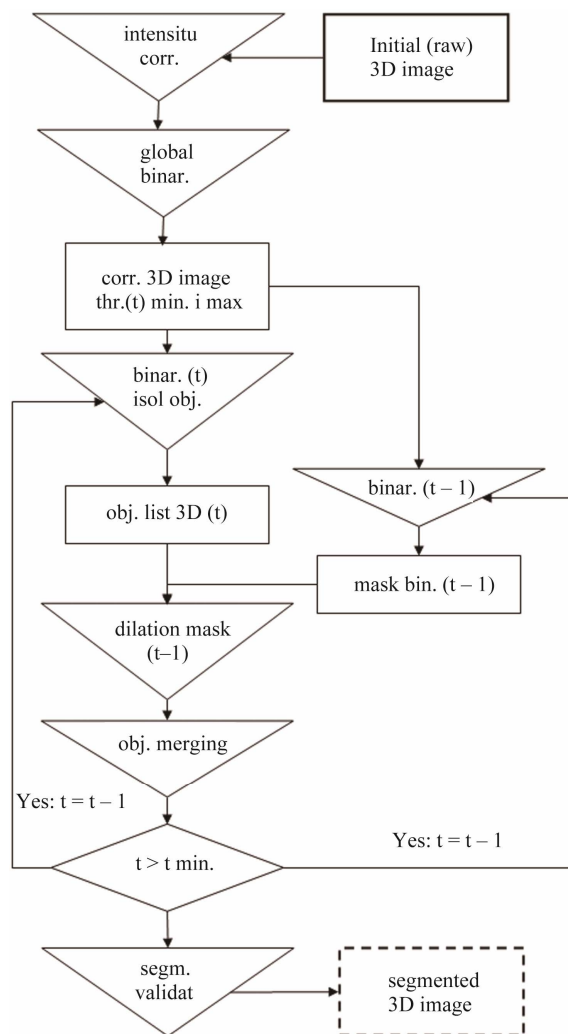
Figure 1. Schematic diagram of the segmentation algorithm. Minimum and maximum values of global binarization threshold (t) are calculated using Otsu algorithm (see Materials and Methods). Input (raw) and output (segmented) 3D images correspond to Figures 2(A), (B) and Figures 2(E), (F), respectively.

Figure 2. 3D image corresponding to input (A, B), intermediate (C, D) and output (E, F) stages of the image segmentation algorithm. The images represent xy (A, C, E) or xz (B, C, D) projections of the 3D data set. Segmented separate volumes (single nuclei or groups of merged nuclei) are color-coded (panels C-F). The axes (Cartesian coordinate system) are shown as green (x), red (y) and blue (z) edges of the data volume. Scale bars (white edges): 10 um.

executed starting from the largest new group and continued until no groups were left to merge. The threshold was then lowered and the whole procedure repeated until the minimum intensity was reached. The objects which were touching the border were excluded from the data set. Similarly, the objects too small (volume below 20000 voxels) to represent whole nuclei were discarded. Finally result of segmentation was validated by a human observer (**Figures 2(E)**, **(F)**).

Sets of resulting binary masks (belonging to correctly isolated interphase nuclei) were used to calculate several morphological parameters with original (uncorrected) image data as the second input. A set of parameters (calculated for each nucleus) included: the shape parameters (volume, linear dimensions, circularity), the global chro-matin fluorescence (DAPI) intensity distribution measures (mean, variance, skewness) and the local distribution parameters of chromatin fluorescence intensity (Haraclick features, wavelet energy, run-length features). The Haralick (gray level co-localization matrix, GLCM) features (parameters) included: variance, entropy, contrast, sum of squares, correlation and homogeneity [32, 33]. The GLCM parameters were calculated on the distances corresponding to: 3, 6, 9, 12, 15 and 18 pixels (from 210 to 1260 nm in xy direction, respectively). The wavelet (Haar) decomposition was calculated on 3 decomposition levels, whereas each level corresponded to 7 sub-bands (application of either low- or high-pass filter in each of 3 dimensions). Therefore, the analyzed details corresponded to 2 - 8 pixels or 140 - 560 nm spatial distance in the xy direction (see **Table 1**). The average (computed over volume of a nucleus) absolute amplitude

Table 1. Sizes of the details (in nm) corresponding to 1st and 2nd levels of the wavelet transform. The respective sub-bands were constructed by application of either low-pass (L) or high-pass (H) filter in x, y, or z directions, respectively.

Transf. tub-band	filtering direction	Transf. level 1		Transf. level 2	
		Min	Max	Min	Max
	x	0	140	140	280
HHH	y	0	140	140	280
	z	0	420	420	880
	x	0	140	140	280
HHL	y	0	140	140	280
	z	420	880	880	1760
	x	0	140	140	280
HLH	y	140	280	280	560
	z	0	420	420	880
	x	140	280	280	560
LHH	y	0	140	140	280
	z	0	420	420	880
	x	0	140	140	280
HLL	y	140	280	280	560
	z	420	880	880	1760
	x	140	280	280	560
LHL	y	0	140	140	280
	z	420	880	880	1760
	x	140	280	280	560
LLH	y	140	280	280	560
	z	0	420	420	880

was used as the energy estimator. The run-length (RL) features were calculated in the xy plane (in directions corresponding to 0, 45, 90, and 135 degrees with respect to the x axis of the dataset) and comprised: fractions of short and long runs, gray level non-uniformity, run-length non-uniformity, and fraction of pixels in runs [32, 34]. In total, 113 parameters characterizing local intensity distribution were calculated for each nucleus. The segmentation and calculation of the parameters were implemented under Matlab R2007b (The MathWorks Inc., Maryland, USA).

The sets of parameters corresponding to populations of nuclei with different number of B-chromosomes (0, 1, 2 or 3) were subjected to discriminant analysis using a binary decision tree (classification and regression trees, C&RT) method [35]. The exhaustive search of the parameter space was used and the quality of fit was estimated with Gini's coefficient. The tree was pruned using classification error and the parameters were ordered with respect to their discriminative power. Subset of parameters constituting optimum classifier for nuclei with different numbers of B-chromosomes was isolated. The classifier was used as an exploratory technique to assist

biological interpretation of the elements (parameters) which contribute to the change of the chromatin distribution (texture) in the presence of B chromosomes. Hence, these parameters were correlated with depth in tissue at which a given nucleus was positioned. This step made it possible to explore magnitude of differences in those texture elements which contributed to the differences in chromatin distribution. Furthermore, the absence of classification artifacts caused by the loss of apparent optical resolution (manifested with image blurring) could be ascertained. The statistical analysis was carried out using Statistica 6.0 (StatSoft, Poland).

3. Results

3.1. Isolation of the Significant Parameters

The parameters characterizing local fluorescence intensity (chromatin) distribution were subjected to discriminant analysis (see Methods) to isolate the set of features which were distinct for nuclei containing different numbers of B chromosomes (from 0 to 3). The decision tree, constructed using the full set of 113 parameters, contained 33 nodes (decisions) and provided 99% overall

classification efficiency (data not shown). Reduction of this tree to 8 nodes (**Figure 3**) demonstrated that the following parameters brought the most significant contribution to the classification: the correlation (GLCM features), the wavelet energy (1 and 2 level of decomposition), the long run emphasis and the fraction of pixels in runs (run-length features, 0 and 90 degrees). These parameters were analyzed in details as described further. The reduced tree provided overall 65% percent classification (**Table 2**). One note that the largest probabilities of misclassification corresponded to discrimination between nuclei containing 2 versus 3 and 1 versus 2 B chromosomes, respectively.

3.2. The GLCM Parameters

The GLCM (Haralick) correlation brought the most significant contribution to the classification of nuclei containing different numbers of B chromosomes. The correlation (representing average of pairs of pixels separated by a given distance) decreases with increasing difference between respective pixel intensities [33]. In other words, the correlation is high when the intensity distribution is uniform (no pattern) and low when intensity non-uniformity (granular pattern) occurs. The sum entropy is minimal when the sum of intensities of pixel pair may accept only one value and maximal when all the possible

values of this parameter are equally probable. The average difference is a measure of absolute difference of intensities of pixel pair. These two parameters reflect regularity of texture pattern.
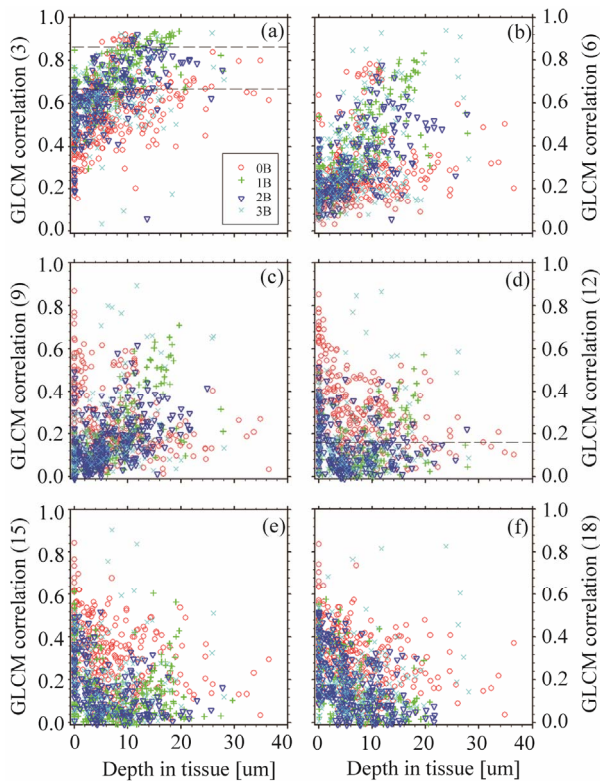
In the nuclei of *C. capilaris* the GLCM correlation measured at the distance of 3 pixels (210 nm) was high and increased with the depth at which a nucleus was positioned in the tissue (**Figure 4(a)**). The nuclei containing no B chromosomes exhibited higher values of this parameter compared to their counterparts carrying from 1 to 3 Bs. One may note that the correlation measured at this distance was similar for all the nuclei containing B chromosomes. The same pattern appeared at the 6 pixel (420 nm) distance (**Figure 4(b)**), although the difference between nuclei devoid of (0 B) and containing B chromosomes (1 B, 2 B and 3 B) was smaller. Here, too, the values increased with the depth. No significant difference between those two classes of nuclei was detectable at 9 pixel distance (630 nm, **Figure 4(c)**). However, the values of the GLCM correlation measured at 12 and 15 pixel distance (840 nm and 1050 nm, respectively) were higher in nuclei containing B chromosomes than in their 0 B counterparts (**Figures 4(d)** and **4(e)**). It may be noted that the difference between these two groups of nuclei studied at the 18 pixel distance (1260 nm) is smaller than in two previous cases (**Figure 4(f)**).

Table 2. Confusion (error) matrix for classification of the nuclei with reduced (8 nodes) binary decision tree. True classes are given in columns whereas the estimated in rows of the table. The absolute numbers corresponding to misclassified nuclei were normalized to the respective numbers of nuclei in classes to give the probability of misclassification (the values in cells).

	0 B	1 B	2 B	3 B
0 B	0	0.103	0.052	0.079
1 B	0.071	0	0.268	0.074
2 B	0.085	0.043	0	0.333
3 B	0.017	0.044	0.286	0
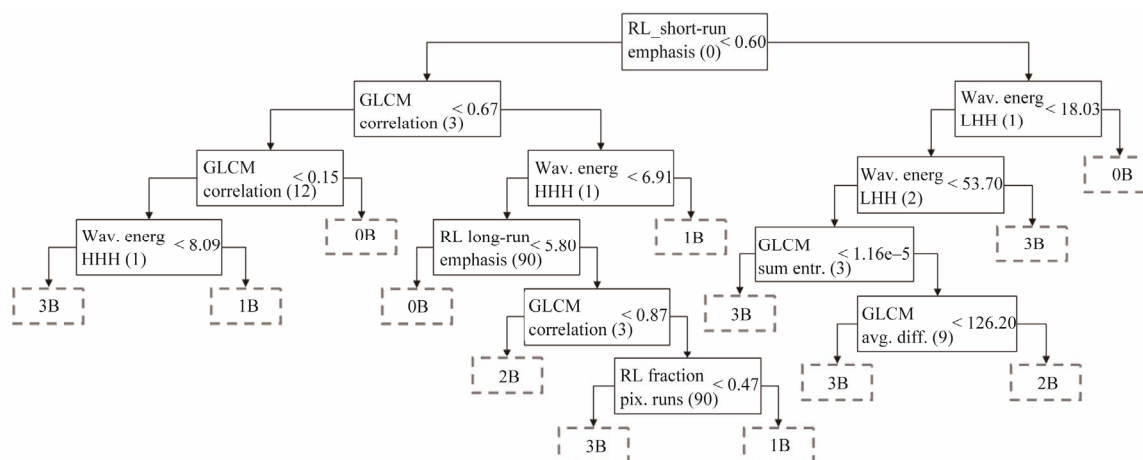
Figure 3. The reduced binary decision tree (CR&T algorithm). The tree nodes are marked with boxes. The names of the parameters used to make binary decisions are shown (with their threshold values) in the boxes. A decision corresponds to choice between the right-hand branch of the tree (if the respective condition is met) and the left-hand branch (otherwise).
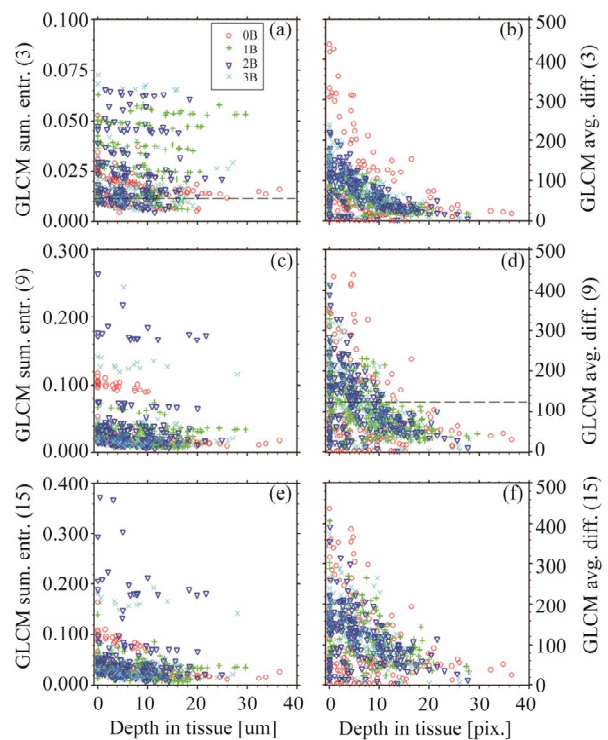
Figure 4. The values of GLCM correlation as a function of position (depth in the tissue) of 0 B (red circles), 1 B (green crosses), 2 B (blue triangles) and 3 B (cyan crosses) nuclei of *C. capilaris*. The values correspond to the distances of: 3 pixels (210 nm, a), 6 pixels (420 nm, b), 9 pixels (630 nm, c), 12 pixels (840 nm, d), 15 pixels (1050 nm, e) and 18 pixels (1260 nm, f). Dashed lines mark respective decision thresholds of the classification tree.

Figure 5. The values of GLCM sum enthropy (a, c, e) and GLCM average difference (b, d, f) as a function of position (depth in the tissue) of 0 B (red circles), 1 B (green crosses), 2 B (blue triangles) and 3 B (cyan crosses) nuclei of *C. capilaris*. The values correspond to the distances of: 3 pixels (210 nm, a, b), 9 pixels (630 nm, c, d) and 15 pixels (1050 nm, e, f). Dashed lines mark respective decision thresholds of the classification tree.

The GLCM sum entropy measured at 3 pixel distance (210 nm, **Figure 5(a)**) was larger in 3 B than in 2 B nuclei. On the other hand the GLCM average sum measured at 9 pixel distance (630 nm, **Figure 5(d)**) was lower in the former than in the latter class (see also **Figure 3**). No other differences between 0 B, 1 B, 2 B and 3 B were detectable using this parameter.

It may be concluded that the chromatin in nuclei devoid of B chromosomes was arranged in small size blocks (210 nm - 420 nm). On the other hand the chromatin in nuclei containing from 1 to 3 of those accessory chromosomes contained larger blocks of chromatin (840 nm - 1050 nm). It is likely that the differences between nuclei carrying from 1 to 3 B chromosomes were minor and connected with regularity of the chromatin distribution pattern.
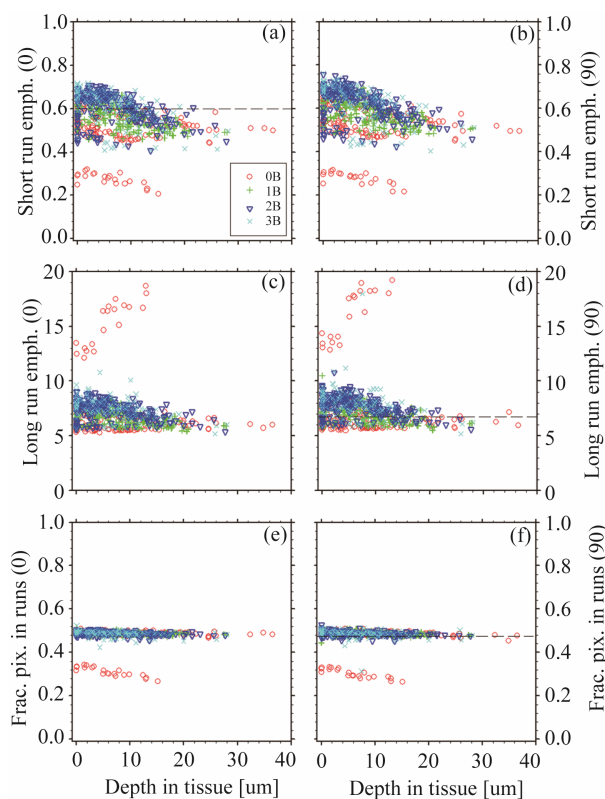
3.3. The Run-Length Parameters

The short- and long-run emphases are measures of prevalence of short and long runs of identical pixels in the set all runs detectable in a nucleus. Fraction of runs re-

flects the content of pixels which are arranged in runs (long and short, 34).

One may note that, using the short-run emphasis two fractions could be distinguished in each of the analyzed populations of the nuclei (containing different numbers of B chromosomes). The values of this parameter were low in the 0 B nuclei compared with their counterparts with the supernumerary chromosomes (**Figures 6(a)**, **(b)**). No significant differences were observed between the latter populations (containing 1 B, 2 B or 3 B). It should be noted that the values of this parameter decreased with the depth at which a nucleus was positioned in the tissue. The two fractions of 0 B nuclei were also detectable with the long-run emphasis (**Figures 6(c)**, **(d)**). However, the values of this parameter in the 0B nuclei were higher (the first fraction) or similar (the second fraction) compared to the respective values of the nuclei containing B chromosomes (**Figures 6(c)**, **(d)**). These two fractions were not detectable in any of the latter classes of nuclei (**Figures 6(c)**, **(d)**). The values of the long-run emphasis were not affected by the position of nucleus in tissue, with the exception of the first fraction (0 B nuclei) where the values increased with the depth. Analysis of the values of

Figure 6. The values of run-length parameters of texture: short run emphasis (a, b), long run emphasis (c, d) and fraction of pixels in runs (e, f) as a function of position (depth in the tissue) of 0 B (red circles), 1 B (green crosses), 2 B (blue triangles) and 3 B (cyan crosses) nuclei of *C. capilaris*. The run-length parameters were calculated in directions corresponding to at 0 (ACE) and 90 (BDF) degrees. Dashed lines mark respective decision thresholds of the classification tree.

the fraction of pixels in runs indicated the existence of the two groups of 0 B nuclei (**Figures 6(e)**, **(f)**). However, similar two groups were not detectable in 1 B, 2 B or 3 B nuclei. The values of the long-run emphasis were not significantly affected by the position of the majority of nuclei in tissue (**Figures 6(e)**, **(f)**). A decrease with depth was observed only in one fraction of nuclei containing no B chromosomes.

One may hypothesize that the nuclei devoid of accessory chromosomes exhibited smaller regularity of chromatin texture (and thus its spatial distribution) than their counterparts containing 1 B, 2 B or 3 B. Furthermore, the difference between two fractions of nuclei was the most pronounced in the former class.
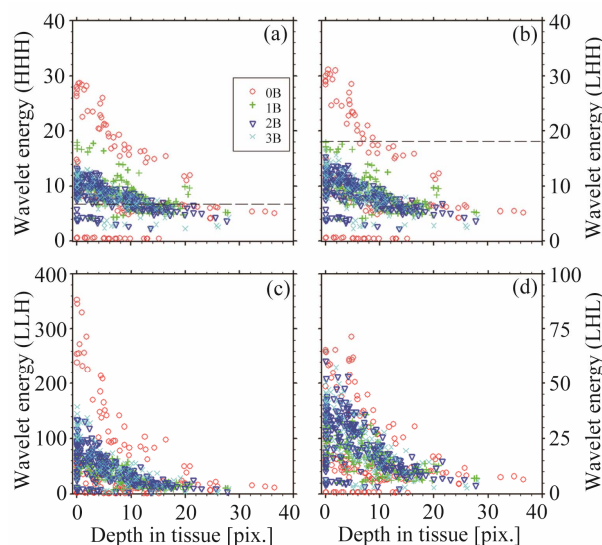
3.4. Wavelet Energy

The nuclei carrying from 0 to 3 B chromosomes exhibited differences with respect to their chromatin texture quantified using the wavelet energy on 1 and 2 levels of decomposition (see Materials and Methods). These data

indicate the presence of two groups of nuclei (0 B, 1 B, 2 B and 3 B). The first of these groups was characterized by higher whereas the second by lower energy in all the sub-bands of the 1 decomposition level (**Figure 7**). One should note that the difference between those two classes was the most pronounced in the population of 0B nuclei (red symbols), less in 1 B (green symbols) and the least pronounced in populations of 2 B and 3 B nuclei (blue and cyan symbols, respectively). The values of the wavelet energy decreased with the depth at which a nucleus was positioned in the tissue. Nonetheless, they tended to be larger for nuclei devoid of the supernumerary chromosomes than in the nuclei carrying those (**Figure 7**). The two groups of nuclei were also observed when the energy corresponding to the second level of decomposition was analyzed (**Figure 8**). The difference in the energy between those groups was largest in the case of 0 B whereas lower values of this parameter were measured in the nuclei containing accessory chromosomes. The wavelet energy decreased with the depth in tissue as well (**Figure 8**).

The analysis of the wavelet energy indicates that the chromatin of the nuclei devoid of B chromosomes contained more small blocks (<560 nm in xy direction) than chromatin of the 1 B, 2 B or 3 B nuclei.

4. Discussion

The distribution of chromatin in the nuclei of *C. capilaris* was visualized using DAPI as fluorescent DNA stain.

Figure 7. The values of the wavelet energy (1st decomposition level) as a function of position (depth in the tissue) of 0B (red symbols), 1 B (green), 2 B (blue) and 3 B (purple) nuclei of C. Capilaris. The energy corresponds to HHH (a); LHH (b); LLH (c) and LHL (d) sub-bands of the wavelet transform. Dashed lines mark respective decision thresholds of the classification tree.
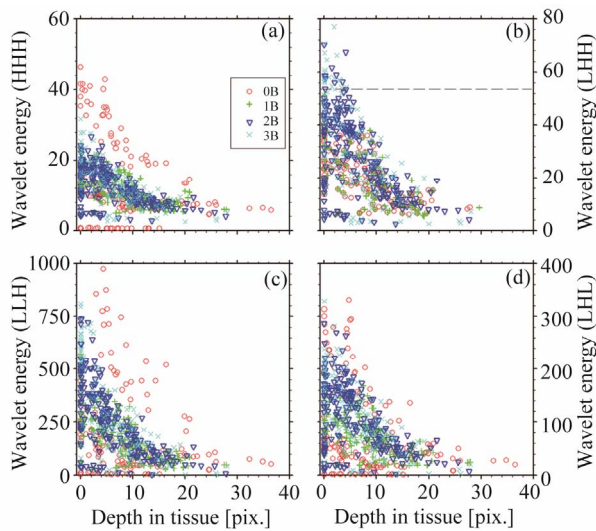
Figure 8. The values of the wavelet energy (2nd decomposition level) as a function of position (depth in the tissue) of 0B (red symbols), 1B (green), 2B (blue) and 3B (purple) nuclei of *C. capilaris*. The energy corresponds to HHH (a); LHH (b); LLH (c) and LHL (d) sub-bands of the wavelet transform. The dashed line marks respective decision thresholds of the classification tree.

The dye has the advantages of being stoichiometric [36], and having low affinity for RNA. Nonetheless, DAPI may exhibit non-uniform binding to DNA strand as the affinity for the regions rich in AT pairs it greater than for the regions rich in GC pairs [37,38]. This preferential binding is used to identify condensed (mitotic) chromosomes with their characteristic banding pattern [39,40]. It should be noted that intensity contrast between AT and GC bands in mitotic chromosomes of *C. capilaris* (DAPI staining) is much lower than between the dim and bright chromatin texture elements in the interphase nuclei (data not shown). On the other hand similar chromatin texture was observed in the nuclei stained with propidium iodide, a dye which does not exhibit the preferential binding. Thus, one may assume that the observed non-uniformity of fluorescence (texture) in the nuclei was not an artifact and reflected non-uniform chromatin distribution.

It should be noted that refractive index of analyzed plant may be different from that of water (*i.e.* mounting medium) and is in general non-uniform owing to the presence of cellular structures (ex. cell walls). Therefore, light micrograhs of nuclei in this tissue were affected by light scattering and absorption (resulting in loss of image contrast) as well as optical aberrations (leading to image distortion). As a consequence, decrease in practical (achievable) microscope resolution with depth in the tissue was observed. This effect was reflected in texture of nuclear images (studied with mathematical measures). One might attempt to eliminate this effect with image deconvolution. However, no standard existed to ascertain

that such attempt was successful and did not produce artifacts of its own. Thus, the values of texture parameters were studied with respect to the position (depth) of the respective nuclei in the tissue. This approach confirmed that differences in texture were observed between nuclei carrying different number of B chromosomes but positioned at the same depth in tissue. Therefore, the differences detectable between populations with C&RT classifier might not result from the nuclei positioned at different depths within the meristem in these populations. One may also note that the nuclei positioned near the surface of the tissue tended to be bigger than their counterparts at greater depth. However, by the same token, this fact did not render the differences between the 0 B, 1 B, 2 B and 3 B populations artifactual. It should be noted that the differences in nuclear texture between these populations were also apparent on visual examination.

The changes in chromatin architecture (monitored with the texture parameters) reflect transition between its condensed and relaxed form (eu- and heterochromatin). The content of these chromatin fractions in nuclei of *C. capilaris* has not been determined exactly. However, judging by the extent of the areas strongly stained with DAPI in mitotic chromosomes (C-band pattern), one may estimate that heterochromatin content of these chromosomes may approach 30% (data not shown). Molecular studies demonstrated that heterochromatin (histones H3 methylated at lysine 9) is present also outside of C-bands in these chromosomes [41]. On the other hand single B chromosome of *Crepis capillaris* may contain over 30% of heterochromatin [10]. The results of the former study [41] agree with this notion indicating that euchromatin content of these chromosomes is approximately 60% while a block of inactive chromatin is present in centromer and pericentromeric region. It should be noted that studies of mitotic chromosomes are based only on visible differences between constitutive heterochromatin and euchromatin and may not provide exact estimate of interphase heterochromatin which also includes facultative heterochromatin. Nonetheless, one might still hypothesize, that the differences in chromatin texture reflect simply the increase in heterochromatin content with increasing number of B chromosomes. If that was the case the greatest difference between 0 B and 3 B might be expected, whereas the differences between 0 B and 1 B, 1 B and 2 B, 2 B and 3 B should be smaller and similar (in magnitude) to one another. This was not observed, as the differences were the most pronounced between nuclei devoided of and containing accessory chromosomes, whereas smaller between all the classes belonging to the latter group.

The presented results were obtained using organ culture. This approach made it possible to obtain large quantities of biological material (meristem tissue) with dif-

ferent (and stable) numbers of B chromosomes. These requirements could not be met in practice when actual plant seeds were used to grow seedlings. Nonetheless, one might hypothesize that some aspects of cell biology were affected by the long-term tissue culture conditions. The presented work is focused on only one such aspect, namely the impact of the presence of different numbers of B chromosomes on nuclei architecture. One should note that *C. capillaris* is nonpolysomatic plant with very simple karyotype (6 chromosomes in the A set). Thus, this organism was found to be cytologically quite stable even in long term culture conditions [42,43]. No major chromosomal aberrations were detectable in our material using DAPI/CMA3 banding. The fact that the cells used to obtain the presented data were able to divide is in agreement with this notion. Furthermore, similar data were obtained using the material delivered from seeds (0 B and 1 B, data not shown). Consequently, it seems unlikely that the culturing affected the results of this study (comparison between nuclei with and without B chromosomes). Nonetheless, it may be hypothesized that the observed effects were a result of minor mutations of the A genome. One should note that the magnitude of changes of chromatin structure followed the number of B chromosomes in systematic manner which renders this possibility unlikely. Thus, presented data indicate that alterations of 3D chromatin distribution occur globally in the interphase nuclei in the presence of Bs. The changes were large enough be detected with the resolution scale provided by light microscopy (*i.e.* significant in comparison with the nucleosome size). The impact of B chromosomes on organization of the chromatin of the A chromosome set was previously reported by other workers [7-9]. It should be noted that only specific (rDNA) chromatin regions in squashed nuclei were investigated due to the constraints of 2D microscopy. The presented data indicate that these effects may not be unique to rDNA but constitute a more general mechanism of modulation of chromatin structure (and its activity).

5. Conclusion

In this paper we present an evaluation of the impact of B chromosome presence on the global interphase nucleus architecture. Basing on image processing and extended image analysis framework we created an algorithm enabling us to measure the differences between nuclei with different B chromosome numbers. The analysis were conducted on nuclei visualized in DAPI stained root meristems, allowing us to avoid the bias connected with severe staining procedures and nuclear isolation. Calculated parameters provided evidence for significant difference between nuclei from populations with different B numbers. Observed changes were specific, B number dependent and were not a simple result of the heterochro-

matin volume incensement. Thus, we provide evidence for the impact of B chromosome presence on the global chromatin condensation pattern.

6. Acknowledgements

REFERENCES

[1] A. Muntzing, "Accesory Chromosomes," *Accessory Chromosomes*, Vol. 8, 1974, pp. 243-266. doi:10.1146/annurev.ge.08.120174.001331

[2] J. P. M. Camacho, T. F. Sharbel and L. Beukeboom, "B-Chromosome Evolution," *Philosophical Transactions B*, Vol. 355, No. 1394, 2000, pp. 163-178. doi:10.1098/rstb.2000.0556

[3] R. N. Jones, "Tansley Review No. 85; B Chromosomes in Plants," *New Phytologist*, Vol. 131, No. 4, 1995, pp. 411-434. doi:10.1111/j.1469-8137.1995.tb03079.x

[4] E. L. Maistro, C. Oliveira and F. Foresti, "Cytogenetic Analysis of A- and B-Chromosomes of *Prochilodus lineatus* (Teleostei, Prochilodontidae) Using Different Restriction Enzyme Banding and Staining Methods," *Genetica*, Vol. 108, No. 2, 2000, pp. 119-125. doi:10.1023/A:1004063031965

[5] V. A. Trifonov, P. L. Perelman, S.-I. Kawada, M. A. Iwasa, S. I. Oda and A. S. Graphodatsky, "Complex structure of B-Chromosomes in Two Mammalian Species, *Apodemus peninsulae* (Rodentia) and *Nyctereutes procyonoides* (Carnivora)," *Chromosome Research*, Vol. 10, No. 2, 2002, pp. 109-116. doi:10.1023/A:1014940800901

[6] A. G. Burgov, T. V. Karamyshera, E. A. Perepelov, E. A. Elisaphenko, D. N. Rubtsov, E. Warchałowska-Śliwa, H. Tatsuta and N. B. Rubsov, "DNA Content of the B Chromosomes in Grasshop per Podisma kanoi Storozh. (Orthoptera, Acrididae)," *Chromosome Research*, Vol. 15, No. 3, 2007, pp. 315-325.

[7] M. Delgado, L. Moraiscecilio, N. Neves, R. N. Jones and W. Viegas, "The Influence of B Chromosomes on rDNA Organization in Rye Interphase Nuclei," *Chromosome Research*, Vol. 3, No. 8, 1995, pp. 487-491. doi:10.1007/BF00713963

[8] M. Delgado, A. Caperta, T. Ribeiro, W. Viegas, R. N. Jones and L. Morais-Cecilio, "Different Numbers of Rye B Chromosomes Induce Identical Compaction Changes in Distinct A Chromosome Domains," *Cytogenetic and Genome Research*, Vol. 106, No. 2-4, 2004, pp. 320-324. doi:10.1159/000079306

[9] L. Morais-Cecilio, M. Delgado, R. N. Jones and W. Viegas, "Modification of Wheat rDNA Loci by the Rye B Chromosomes, a Chromatin Organization Model," *Chromosome Research*, Vol. 8, No. 2-4, 2000, pp. 341-351. doi:10.1023/A:1009291714371

[10] J. Maluszynska and D. Schweizer, "Ribosomal RNA Genes in B Chromosomes of *Crepis capillaries* Detected

by Non-Radioactive *in Situ* Hybridization," *Heredity*, Vol. 62, 1989, pp. 59-65. doi:10.1038/hdy.1989.8

[11] M. Gonzalez-Sanchez, M. Chiavarino, G. Jimenez, S. Manzanera, M. Rosato and M. J. Puertas, "The Parasitic Effects of Rye B Chromosomes Might Be Beneficial in the Long Term," *Cytogenetic and Genome Research*, Vol. 106, No. 2-4, 2004, pp. 386-393. doi:10.1159/000079316

[12] R. N. Jones, "B-Chromosome Systems in Flowering Plants and Animal Species," *International Review of Cytology*, Vol. 40, 1975, pp. 1-100. doi:10.1016/S0074-7696(08)60951-1

[13] C. R. Leach, A. Houben and J. N. Tinnis, "The B Chromosomes in Brachycome," *Cytogenetic and Genome Research*, Vol. 106, No. 2-4, 2004, pp. 199-209. doi:10.1159/000079288

[14] R. T. Grant-Downton and G. Dickinson, "Epigenetics and Its Implications for Plant Biology. 1. The Epigenetic Network in Plants," *Annals of Botany*, Vol. 96, No. 7, 2005, pp. 1143-1164. doi:10.1093/aob/mci273

[15] P. Fransz, W. Soppe and I. Shubert, "Heterochromatin in Interphase Nuclei of *Arabidopsis thaliana*," *Chromosome Research*, Vol. 11, No. 3, 2004, pp. 227-240. doi:10.1023/A:1022835825899

[16] P. Fransz, R. van Hoopen and F. Tessadori, "Composition and Formation of Heterochromatin in *Arabidopsis thaliana*," *Chromosome Research*, Vol. 14, No. 1, 2006, pp. 71-82. doi:10.1007/s10577-005-1022-5

[17] N. Dillon, "Heterochromatin structure and function," *Biology of the Cell*, Vol. 96, No. 8, 2004, pp. 631-637. doi:10.1016/j.biolcel.2004.06.003

[18] J. A. Fahrner and S. B. Baylin, "Heterochromatin: Stable and Unstable Invasions Home and Abroad," *Genes & Development*, Vol. 17, No. 15, 2003, pp. 1805-1812. doi:10.1101/gad.1123303

[19] M. J. Puertas, "Nature and Evolution of B Chromosomes in Plants: A Non-Coding but Information Rich Part of Plant Genomes," *Cytogenetic and Genome Research*, Vol. 296, No. 1-4, 2002, pp. 198-205. doi:10.1159/000063047

[20] M. V. Boland, M. K. Markey and R. F. Murphy, "Automated Recognition of Patterns Characteristic of Subcellular Structures in Fluorescence Microscopy Images," *Cytometry*, Vol. 33, No. 3, 1998, pp. 366-375. doi:10.1002/(SICI)1097-0320(19981101)33:3<366::AID-CYTO12>3.0.CO;2-R

[21] K. Huang, J. Lin, J. A. Gajnak and R. F. Murphy, "Image Content-Based Retrieval and Automated Interpretation of Fluorescence Microscope Images via the Protein Subcellular Location Image Database," *Proceedings of* 2002 *IEEE International Symposiums on Biomedical Imaging* (*ISBI* 2002), 2002, pp. 325-328. doi:10.1109/ISBI.2002.1029259

[22] A. Huisman, L. S. Ploeger, H. F. J. Dullens, N. Poulin, W. E. Grizzle and P. J. van Diest, "Development of 3D Chromatin Texture Analysis Using Confocal Laser Scanning Microscopy," *Cellular Oncology*, Vol. 27, No. 5-6, 2005, pp. 335-345.

[23] K. C. Strasters, A. W. M. Smenlders, M. Buijs, A. B.

Houtsmuller, H. T. M. van der Voort and N. N. Nanninga, "A 3-D Model for Chromatin Organization of G1 and G2 Populations from Quantitative Confocal Image Analysis," *Cytometry*, Vol. 27, No. 3, 1997, pp. 201-212. doi:10.1002/(SICI)1097-0320(19970301)27:3<201::AID-CYTO1>3.0.CO:2-H

[24] G. Van de Wouwer, B. Weyn, P. Scheunders, W. Jacob, E. van Marck and D. van Dyck, "Wavelets as Chromatin Texture Description for Automated Identification of Neoplastic Nuclei," *Journal of Microscopy*, Vol. 197, No. 1, 2000, pp. 25-35. doi:10.1046/j.1365-2818.2000.00594.x

[25] S. Yatouji, F. Liautaud-Roger and J. Dufer, "Nuclear Chromatin Texture and Sensitivity to DNase I in Human Leukaemic CEM Cells Incubated with Nanomolar Okadaic Acid," *Cell Proliferation*, Vol. 33, No. 1, 2000, pp. 51-62. doi:10.1046/j.1365-2184.2000.00163.x

[26] S. Abraham, I. H. Ames and H. H. Smith, "Autoradiagraphic Studies of DNA Synthesis in the B Chromosomes of *Crepis capillaries*," *Journal of Heredity*, Vol. 59, No. 5, 1968, pp. 297-299.

[27] J. Juchimiuk and J. Maluszynska, "Transformed Roots of *Crepis capillaries*—A Sensitive System for the Evaluation of the Clastogenicity of Abiotic Agents," *Mutation Research*, Vol. 565, No. 2, 2005, pp. 129-138. doi:10.1016/j.mrgentox.2004.10.016

[28] P. F. Ambros, M. A. Matzke and A. J. M. Matzke, "Detection of a 17 kb Unique Sequence (T-DNA) in Plant Chromosome by *in Situ* Hybridization," *Chromosoma*, Vol. 94, No. 1, 1986, pp. 11-18. doi:10.1007/BF00293525

[29] J. Maluszynska, "The Effect of B Chromosomes and T-DNA on Chromosomal Variation in Callus Cells and Regenerated Roots of *Crepis capillaris*," *Plant Cell Tissue Organ Cult*, Vol. 50, No. 2, 1997, pp. 113-118. doi:10.1023/A:1005727529303

[30] N. Otsu, "A Threshold Selection Method from Gray-Level Histograms," *IEEE Transactions on Systems*, *Man and Cybernetics*, Vol. 9, No. 1, 1979, pp. 62-66. doi:10.1109/TSMC.1979.4310076

[31] M. Sezgin and B. Sankur, "Survey over Image Thresholding Techniques and Quantitative Performance Evaluation," *Journal of Electronic Imaging*, Vol. 13, No. 1, 2004, pp. 146-165. doi:10.1117/1.1631315

[32] C. J. S. Ferro, "Scale and Texture in Digital Image Classification," Ph.D. Desideration, Eberly Collage of Arts and Sciences at West Virginia University, 2003.

[33] M. Tuceryan and A. K. Jain, "Texture Analysis. The Handbook of Pattern Recognition and Computer Vision (2nd Edition)," World Scientific Publishing, 1998, pp. 207-248.

[34] D. H. Xu, A. Kurani, J. D. Furst and D. S. Raicu, "Run-Length Encoding for Volumetric Texture," *The* 4*th IASTED International Conference on Visualization*, *Imaging*, *and Image Processing*, Marbella, 2004.

[35] L. Breiman, J. Friedman, R. Olshen and C. Stone, "Classification and Regression Trees," 1st Edition, Chapman & Hall, London, 1984.

[36] Z. Darzynkiewicz, M. R. Melamed, T. Lindmo and M. R.

Mendelsohn (Eds.), "Flow Cytometry and Sorting," Wiley-Liss Inc., New York, 1990, pp. 315-340.

[37] T. A. Larsen, D. S. Goodsell, D. Cascio, K. Grzeskowiak and R. E. Dickerson, "The Structure of DAPI Bound to DNA," *Journal of Biomolecular Structure and Dynamics*, Vol. 7, No. 3, 1989, pp. 477-491. doi:10.1080/07391102.1989.10508505

[38] G. Manzini, M. L. Barcellona, M. Avitabile and F. Quadrifoglio, "Interaction of Diamidino-2-Phenylindole (DAPI) with Natural and Synthetic Nucleic Acids," *Nucleic Acids Research*, Vol. 11, No. 24, 1983, pp. 8861-8876. doi:10.1093/nar/11.24.8861

[39] D. Schweizer, "Reverse Fluorescent Chromosome Banding with Chromomycin and DAPI," *Chromosoma*, Vol. 58, No. 4, 1976, pp. 307-324. doi:10.1007/BF00292840

[40] M. S. Lin, D. E. Comings and O. S. Alfi, "Optical Studies of the Interaction of 4'-6'-Diamidino-2-Phenylindole with DNA and Metaphase Chromosomes," *Chromosoma*, Vol. 60, No. 1, 1977, pp. 15-25. doi:10.1007/BF00330407

[41] A. Houben, D. Demidov, D. Gernand, A. Meister, C. R. Leach and I. Schubert, "Methylation of Histone H3 in Euchromatin of Plant Chromosomes Depends on Basic Nuclear DNA Content," *Plant Journal*, Vol. 33, No. 6, 2003, pp. 967-973. doi:10.1046/j.1365-313X.2003.01681.x

[42] J. Maluszynska, "B Chromosomes of *Crepis capillaris* (L.) Waller. *In Vivo* and *in Vitro*," Ph.D. Desideration, University of Vienna, Vienna, 1990.

[43] M. D. Sacristan, "Karyotypic Changes in Callus Cultures from Haploid and Diploid Plants of *Crepis capillaris* L., Wallr," *Chromosoma*, Vol. 33, No. 3, 1971, pp. 273-283. doi:10.1007/BF00284945